HERA116
Received: 13 Oct 2022

Cross-feed Correlations as a Probe of Antenna Response Variation

Zachary Martinot

August 2022

1 Introduction

This note describes the potential use of the set of cross-correlations between the two feed polarizations on a single antenna as a sensitive probe of beam variations between different antennas. Unlike visibilities - cross-correlations between feeds of two different antennas - the cross-feed correlation probes an individual antenna in relative isolation from the others, which may allow a cleaner statistical characterization of the antenna variation, as well as having a higher SNR than even the shortest baselines. By additionally utilizing the two auto correlations for each antenna the cross-feed correlation is made independent of the receiver chain effective gains for each feed, and thus the variation in this quantity between antennas should isolate differences in the direction-dependent antenna responses. Of immediate potential use is that variations of the spectrum of a single antenna between different days at a fixed LST may be attributed to changes in that particular antenna on that day. Longer term, the cross-feed correlations may be a useful constraint for models of antenna variation for validation simulations and advanced filtering schemes.

2 Cross-feed Correlation Coefficient

The usual formalism spiel will be useful to establish notation. Let $\mathcal{V}_{abij}(t,\nu) \equiv \mathcal{V}_{ab}(t,\nu,\vec{\mathbf{r}}_i,\vec{\mathbf{r}}_j)$ be the visibility measured by two antenna feeds, feed a of the i'th antenna at position $\vec{\mathbf{r}}_i$, and feed b of the j'th antenna at position $\vec{\mathbf{r}}_j$, observed at time t and frequency ν. Recall the standard description of the visibility $\mathcal{V}$ is the complex-valued function defined by the integrals

$$\mathcal{V}_{ab}(t,\nu,\vec{\mathbf{r}}_i,\vec{\mathbf{r}}_j) = \int_{\hat{\mathbf{s}}\in\mathbb{S}^2} J_a^{\alpha}(\vec{\mathbf{r}}_i,\nu,\hat{\mathbf{s}}) C_{\alpha\beta}(\nu,\hat{\mathbf{s}}'(t,\hat{\mathbf{s}})) J_b^{*\beta}(\vec{\mathbf{r}}_j,\nu,\hat{\mathbf{s}}) e^{-2\pi i \frac{\nu}{c}(\vec{\mathbf{r}}_j-\vec{\mathbf{r}}_i)\cdot\hat{\mathbf{s}}} \tag{1}$$

and the function $J_a^{\alpha}(\vec{\mathbf{r}}_i,\nu,\hat{\mathbf{s}})$ is the electric field response of feed a on antenna i at position $\vec{\mathbf{r}}_i$, that is a complex-vector-valued function for each a. At present we are concerned with the zero-separation "visibilities" (i.e. $\vec{\mathbf{r}}_i = \vec{\mathbf{r}}_j$) and we assume that the phase centers of the two feeds on an single antenna i are effectively on top of each other, so that the spatial fringe factor is unity and the set of four correlation products produced by correlating the signals from the two feeds on a single antenna i is described by

$$\mathcal{V}_{abii}(t,\nu) = \int_{\hat{\mathbf{s}}\in\mathbb{S}^2} J_{ai}^{\alpha}(\nu,\hat{\mathbf{s}}) C_{\alpha\beta}(\nu,\hat{\mathbf{s}}'(t,\hat{\mathbf{s}})) J_{bi}^{*\beta}(\nu,\hat{\mathbf{s}}). \tag{2}$$

The two cross-feed correlation products are redundant but unlike the auto correlations V_{aaii}, the cross-feed correlations may be complex-valued due to any phase differences encoded by the different response functions J_{ai}^{α} for each feed and the equivalence is thus $V_{abii} = V_{baii}^*$. The measured auto correlations also include an additional term due to the auto correlation of the additive noise produced in the receiver chain. This term is however not present in the cross-feed correlation as the noises in each feeds receivers are nominally uncorrelated. The measured correlation products are thus described by

$$\hat{\mathcal{V}}_{abii} = g_{ai} g_{bi}^* (\mathcal{V}_{abii} + \mathcal{V}_{ai}^r \delta_{ab}) \tag{3}$$

where δ_{ab} is the Kronecker delta and $\mathcal{V}_{ai}^r$ and g_{ai} are respectively the receiver power offset and the complex effective gain factor for the feed a. In order to isolate variations in the direction dependent response J_{ai}^{α}

from the gain factors we can define the Cross-feed Correlation Coefficient (CCC) for each antenna i at time t and frequency ν as

$$v_i = \frac{\hat{\mathcal{V}}_{enii}}{\sqrt{\hat{\mathcal{V}}_{eeii}\hat{\mathcal{V}}_{nnii}}} \tag{4}$$

where $a, b \in \{e, n\}$ are the labels for the two feed polarizations of a HERA antenna. Here the gain amplitudes $|g_{ai}|$ have been divided out, however any phase difference $\phi_{ei} - \phi_{ni}$ between the two feeds receiver chains remains, and in terms of the intrinsic visibilities the CCC is

$$v_i = \frac{e^{i(\phi_{ei}-\phi_{ni})}\mathcal{V}_{enii}}{\sqrt{(\mathcal{V}_{eeii} + \mathcal{V}^r_{ei})(\mathcal{V}_{nnii} + \mathcal{V}^r_{ni})}}. \tag{5}$$

The amplitude

$$|v_i| = \frac{|\mathcal{V}_{enii}|}{\sqrt{(\mathcal{V}_{eeii} + \mathcal{V}^r_{ei})(\mathcal{V}_{nnii} + \mathcal{V}^r_{ni})}} \tag{6}$$

is then completely independent of the gains and thus variation in $|v_i|$ between antennas may be attributed to differences in antenna response functions $J^\alpha_{ai}(\nu, \hat{\mathbf{s}})$.

A cursory inspection of any HERA data will show obvious and significant differences between the frequency spectra of the CCC for different antennas. In this work we will inspect some H4C data to provide examples of the characteristics of the cross-feed correlations and CCC. Throughout this note, no processing of the data has been done, no flagging or filtering, nor calibration (which would simply be divided out). The only operations performed are the computation of v_i for each time integration and frequency channel, and some averaging. Additionally, we compare a simulation of the auto/cross-feed correlations computed from the Fagnoni beam model for a single, isolated HERA antenna, the Southern Sky Model as the model of Stoke-I on the sky, and additionally includes a model of the receiver temperature spectrum in the auto-correlations ($\mathcal{V}^r$ in Equation 6) using the expected values quoted in Fagnoni 2021 (section 3).

In Figure 1 we inspect a sampling of the CCC amplitude spectra for a subset of 20 antennas from the H4C data recorded on JD 2459122. The CCC $v_i(\nu, t)$ is computed for each time integration, and then averaged over ~ 1 minute to suppress thermal noise. The CCC does not vary appreciably over such a time span, as we will see in the next section. The thing to note here is that while there are some average common large-scale features, each of the antennas CCC spectrum is different in detail. Since an average gain spectrum has been divided out, the variation is attributable to variations in the direction-dependent response between antennas.

Figure 2 shows the phase for the same.

3 Instrumental Response and Time Dependence

If we assume that the sky polarization is a weak contribution to the auto and cross-feed correlations they can be approximated as

$$\mathcal{V}_{abii}(t, \nu) \approx \int_{\hat{\mathbf{s}}\in\mathbb{S}^2} I(\nu, \hat{\mathbf{s}}'(t, \hat{\mathbf{s}}))D_{abi}(\nu, \hat{\mathbf{s}}), \tag{7}$$

where we define the instrumental response kernel here as

$$D_{abi}(\nu, \hat{\mathbf{s}}) = J^\alpha_{ai}(\nu, \hat{\mathbf{s}})J^{*\alpha}_{bi}(\nu, \hat{\mathbf{s}}). \tag{8}$$

The functions D_{ee} and D_{nn} are the familiar directivity functions for each feed. The function D_{en} is then the inner product between the electric field response functions of the two feeds at each point on the sky.

It is reasonable to be skeptical of the limits of this approximation. After all, an observer interested in measuring polarization properties of astronomical emission might hope that the nominally cross-polarized correlation measurement would be sensitive to polarization on the sky. But aspects of the variation between days suggests polarization contributions are not apparent on the 1-2min integration time scales shown here, see section 4 and section 6.

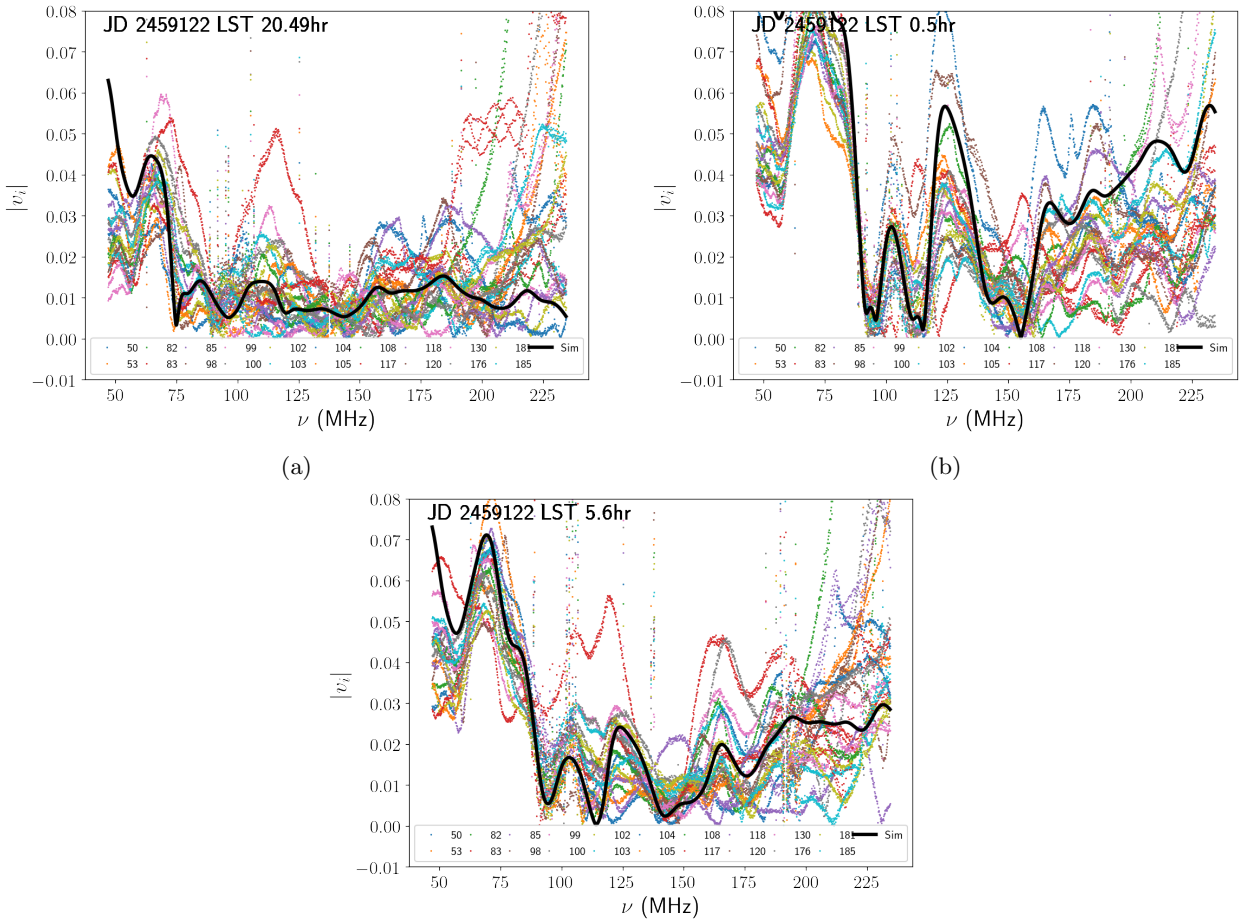

Figure 1: Examples of the amplitude of the CCC, where each curve is the CCC for a different antenna. In these plots the CCC v_i is averaged for ∼1 minute before taking the amplitude.

Figure 3 and Figure 4 show examples of the auto/cross-feed correlation instrumental response kernels where we can see plainly that the D_{en} function is rather different from D_{ee} and D_{nn}. The nulls through the zenith point along the north-south and east-west lines correspond to the points where the two dipole feed have nominally orthogonal responses. The quadrupolar structure and sign changes in the real part is a generic feature of two crossed dipole feeds and for an ideal Hertzian dipole, the imaginary part is identically zero everywhere.

The null point at the zenith means that the cross-feed correlation is most sensitive to a slightly different part of the sky and beam than the autos are. While the autos are dominated by whatever is at zenith, the cross-feeds are most sensitive to an area further out in the beam, perhaps about the half-power point. This means that the spectral structure apparent in the autos and cross-feeds are also dominated by the structure in these different parts of the beam.

The structure of D_{en} is also informative as to what to expect in the time dependence of the CCC. Since there is no fringe, the cross-feed correlation will vary fairly slowly like an auto-correlation. But since D_{en} has an oscilatory structure over the sky, the cross-feed correlation can change a bit faster than an auto as sources move through the qudrupolar structure. Combined with the imaginary part and the character of the cross-feed correlation function $\mathcal{V}_{abii}$ is somewhat inbetween that of an auto-correlation and a visibility. Figure 5 shows how the CCC hardly changes over several minute time scales while Figure 6 then shows how it can vary more quickly over the course of hours than an auto-correlation.

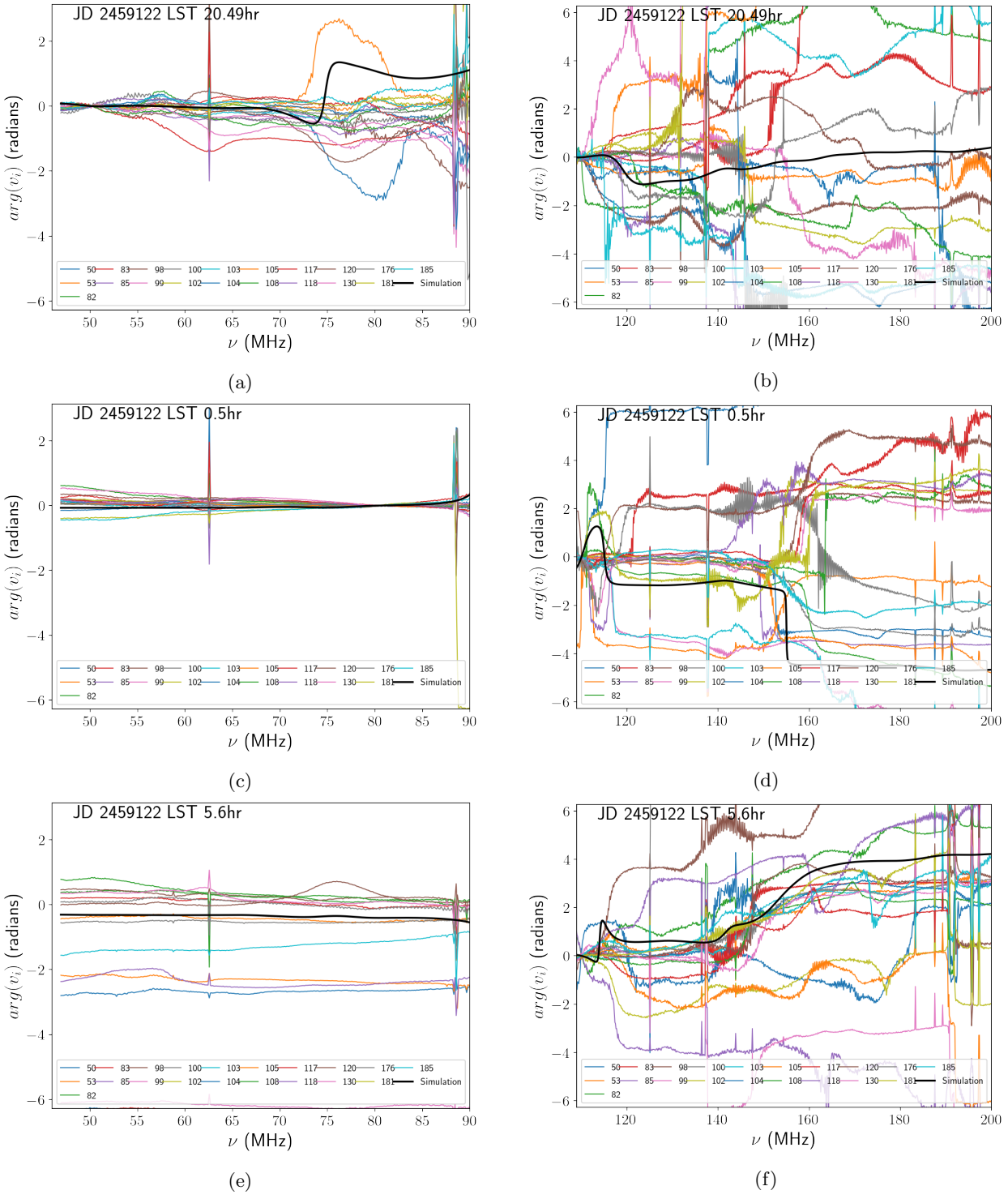

Figure 2: The phase spectra of v_i for the same times and antennas shown in Figure 1. The frequency band is split into a low and high band section with different reference points. Keep in mind that unlike the amplitude, in principle there is a residual direction-independent gain phase.

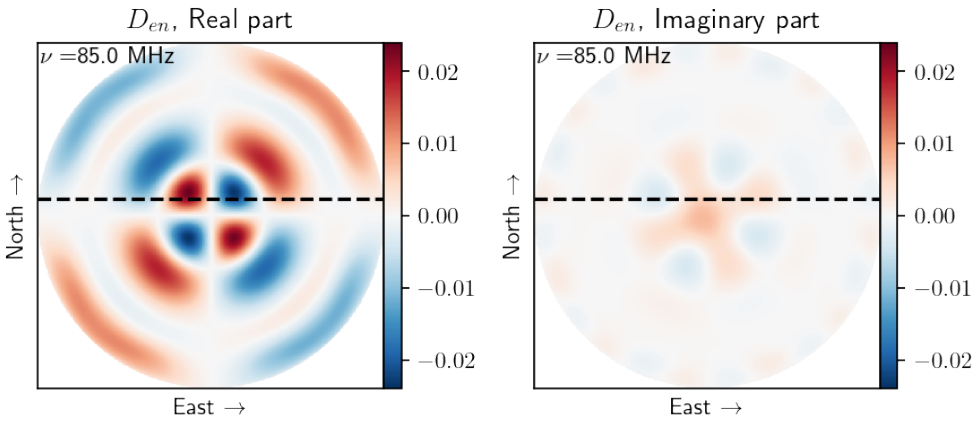

(a)

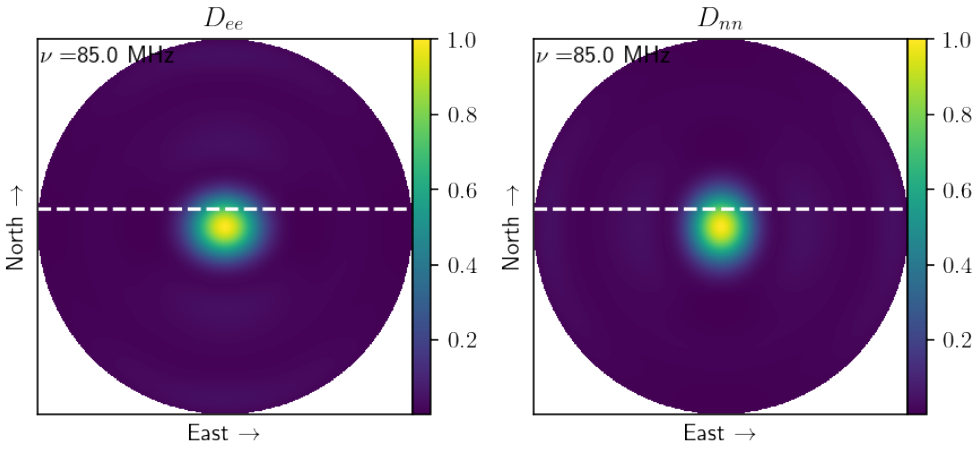

(b)

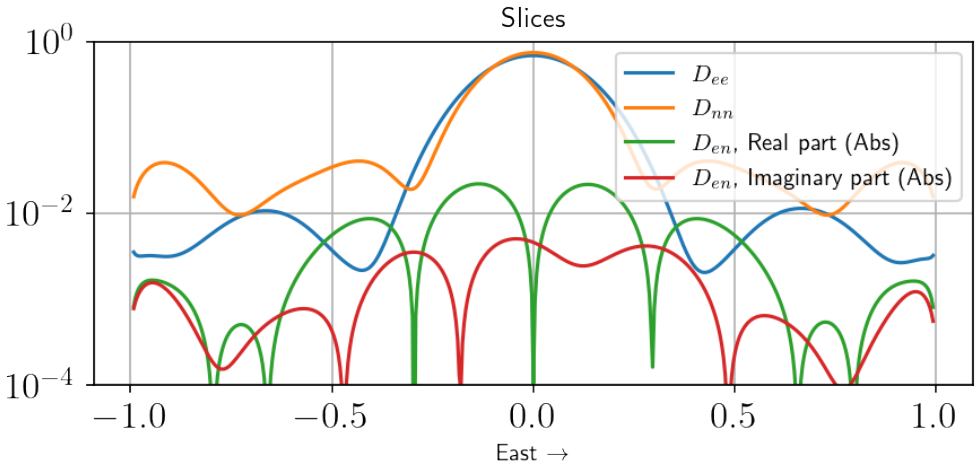

(c)

Figure 3: Orthographic plots of the instrumental response kernels Equation 8 at 85MHz for the auto and cross-feed correlations. The curves in the bottom plot are slices along the dashed lines in the images.

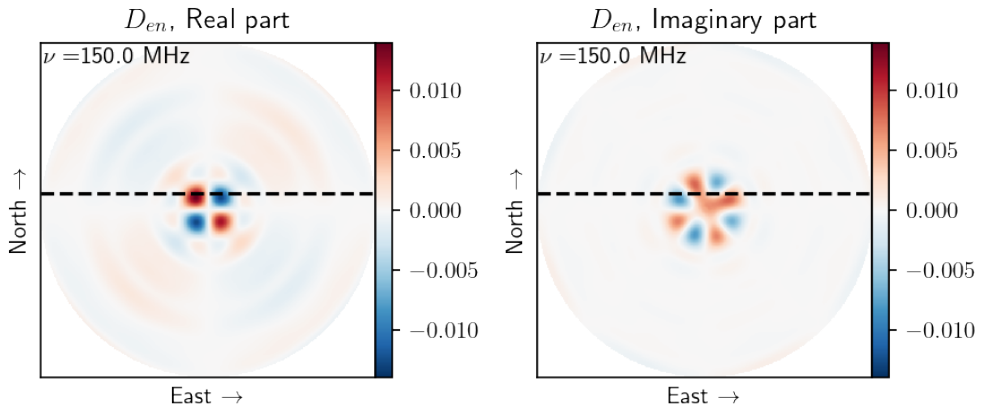

(a)

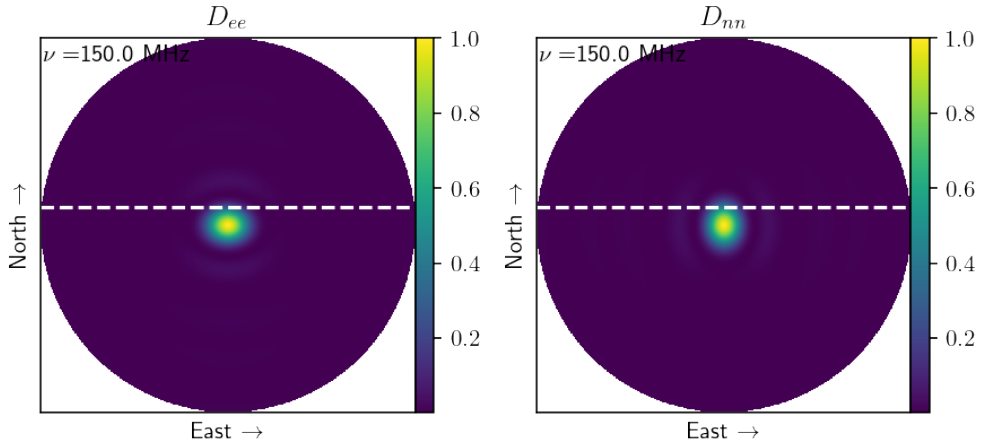

(b)

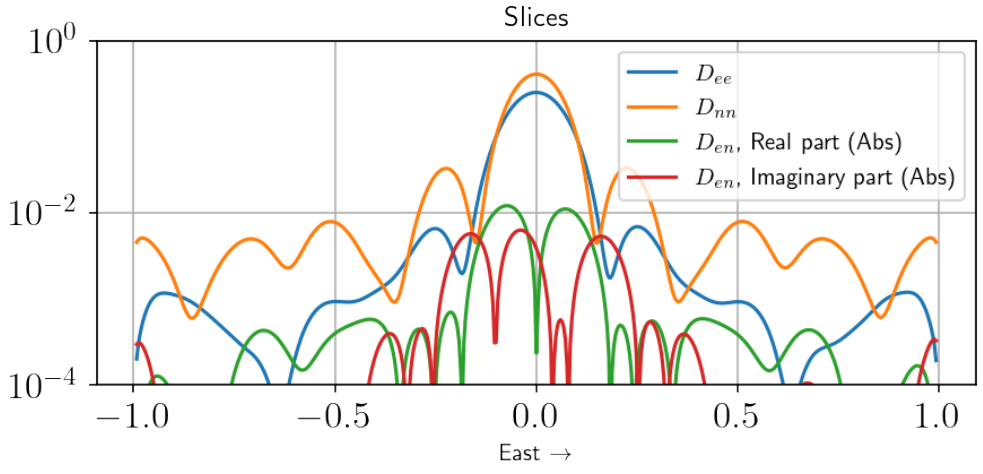

(c)

Figure 4: Orthographic plots of the instrumental response kernels Equation 8 at 150MHz for the auto and cross-feed correlations. The curves in the bottom plot are slices along the dashed lines in the images.

4 Variation Between Days

In Figure 8 - Figure 15 we examine the variation of the CCC for each of 20 antennas over two weeks of H4C. For reference the full set of auto and cross-feed correlation plots are also provided. Here one can see that

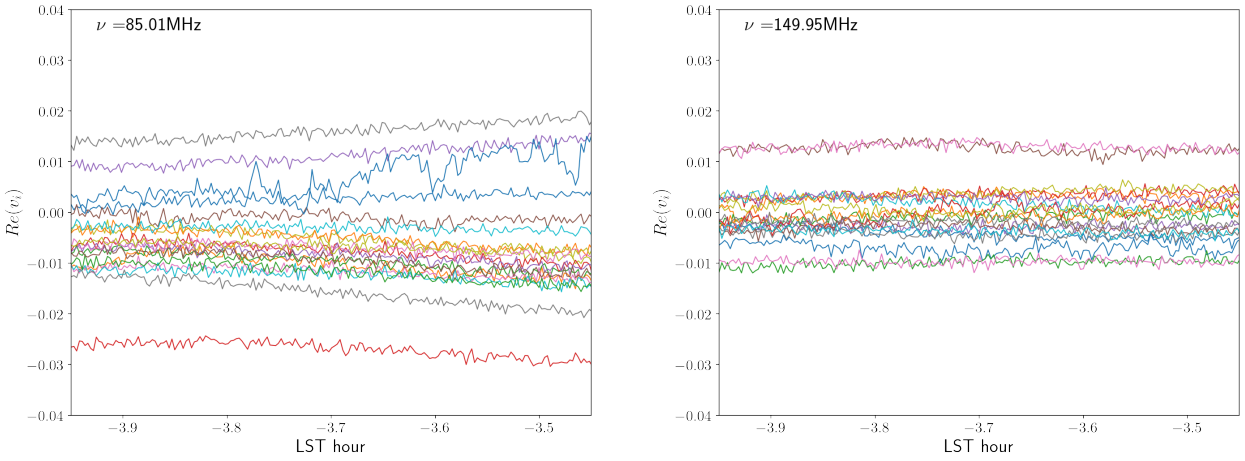

(a) (b)

Figure 5: Raw time series of the CCC for 20 antennas over a half-hour showing the slow variation.

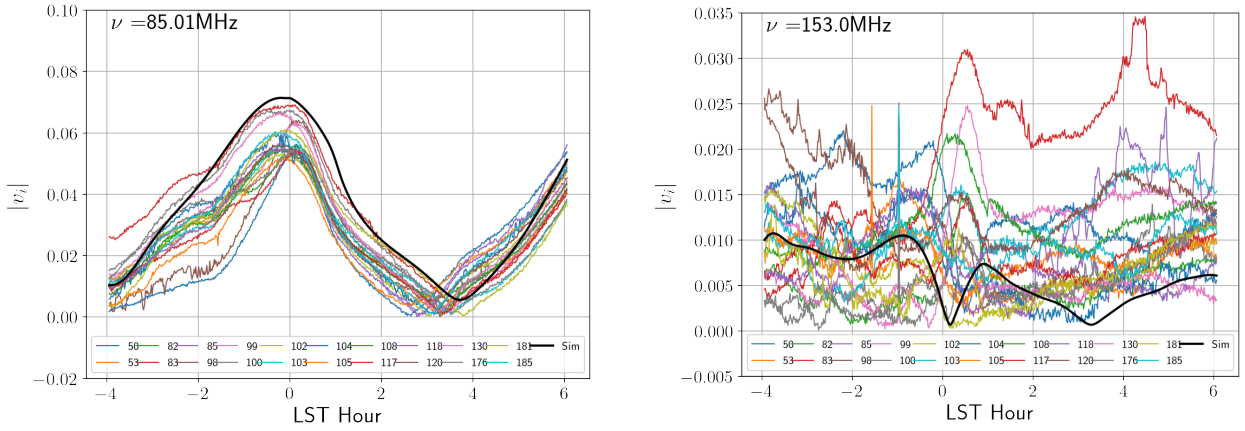

(a) (b)

Figure 6: Time series of the CCC for 20 antennas over a longer range. Here each point is the CCC averaged over 1 minute

the overall gain scale that changes from day to day in the autos is divided out in the CCC by considering for example antennas 102 or 105. Many antennas show consistency over multiple days suggesting that while their gain scales may be flucating from day to day, their beam shapes remain unperturbed as one might hope. On the other hand there is the standout of antenna 117 which shows significant variation in the CCC over the two weeks, while its auto correlations are relatively unremarkable. The hypothesis here is that something was perturbing antenna 117's structure in some way that changed the beam from day to day.

It may thus be useful to track the CCC over time to detect changes in the antennas. On the other hand it remains an open question whether variation such as seen in 117 is actually a problem worth doing something about.

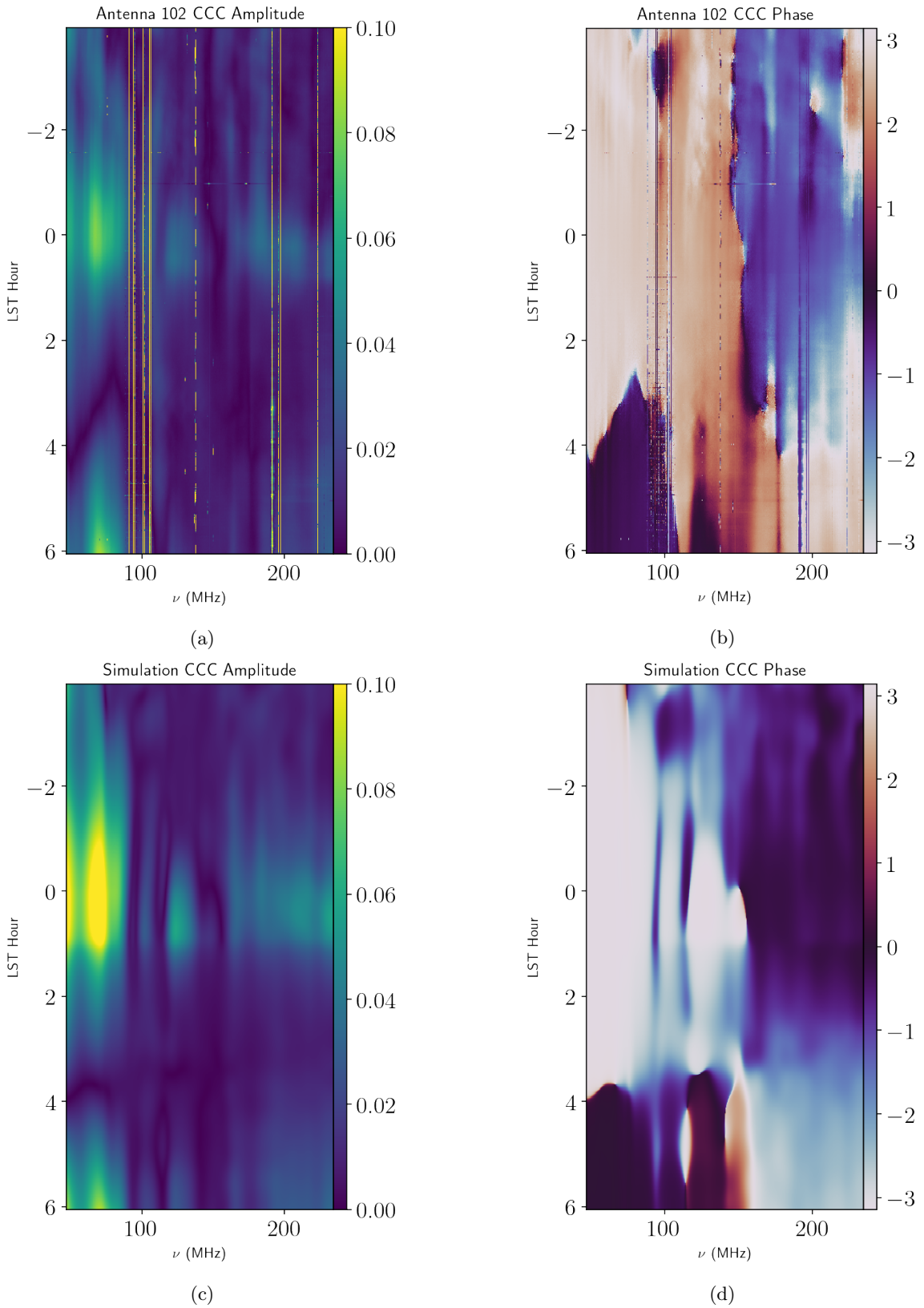

Figure 7: Waterfalls of the amplitude and phase of v_i for antenna 102 on 2459122 and for the simulated v_i.

5 Perturbation Parameterization of Antenna Variations

For any set of N antennas we can define the mean beam as

$$\bar{J}_a^\alpha = \frac{1}{N}\sum_{i=1}^{N} J_{ai}^\alpha. \tag{9}$$

The variation among antenna beams can then be described by an antenna-dependent perturbation to this average beam as

$$D_{ai}^\alpha = J_{ai}^\alpha - \bar{J}_a^\alpha \tag{10}$$

so that the auto/cross-feed correlations are

$$\mathcal{V}_{abii} = \int_{\hat{\mathbf{s}}\in\mathbb{S}^2} \left(\bar{J}_a^\alpha + D_{ai}^\alpha\right) C_{\alpha\beta} \left(\bar{J}_b^{*\beta} + D_{bi}^{*\beta}\right). \tag{11}$$

We might then define an unperturbed auto/cross-feed correlation by

$$\overline{\mathcal{V}}_{ab} = \int_{\hat{\mathbf{s}}\in\mathbb{S}^2} \bar{J}_a^\alpha C_{\alpha\beta} \bar{J}_b^{*\beta} \tag{12}$$

so that the measured auto/cross-feed correlations are then written as

$$\mathcal{V}_{abii} = \overline{\mathcal{V}}_{ab} + \int_{\hat{\mathbf{s}}\in\mathbb{S}^2} D_{ai}^\alpha C_{\alpha\beta} \bar{J}_{bi}^{*\beta} + \int_{\hat{\mathbf{s}}\in\mathbb{S}^2} \bar{J}_a^\alpha C_{\alpha\beta} D_{bi}^{*\beta} + \int_{\hat{\mathbf{s}}\in\mathbb{S}^2} D_{ai}^\alpha C_{\alpha\beta} D_{bi}^{*\beta}. \tag{13}$$

The idea here is that the CCC then serves as a constraint on models of the perturbations $D_{ai}^\alpha(\nu, \hat{\mathbf{s}})$. The significant variations between antennas (e.g. Figure 1) are likely attributable, at least in some large part, to mutual coupling between the closely packed antennas in the HERA array. The first-order scattering approximation presented by Josaitis et al 2022 is an example of a model that could be compared to the data through the measured CCC. The investigation of the effects of feed position errors could be expanded to see how the CCC spectrum changes (see. HERA Memo #105 and Honggeun et al 2022). More generally one might hope to constrain parameters of a covariance model

$$\left\langle D_{ai}^\alpha(\nu, \hat{\mathbf{s}}) D_{bj}^{*\beta}(\nu', \hat{\mathbf{s}}') \right\rangle \tag{14}$$

for the perturbations, which may be part of a better understanding of how to filter/weight the data to mitigate the spectral structure in the antenna beams through the linear decomposition above.

To this end, in Figure 16 we see how the variations between antennas seem to average down to something that is apparently smoother than any individual antenna's spectrum and is better modeled by the simulation which is computed with the beam model of a single HERA dish in isolation.

Of course all this is simply a sketch of a decent chunk of future work, not shown here.

6 Ruling Out Ionospherically Modulated Polarization

A potential confounding factor in the comparison of the cross-feed correlations between days is the polarization of the sky, with it's polarization state modulated by the ionosphere. Since the Faraday rotation induced by the ionosphere can vary from day to day, and the cross-feed correlation is in principle sensitive to the polarization of the sky, it is conceivable that a change in the cross-feed correlation between two different days is due to polarized sky signal instead of a change in the antenna beam. However we can see that this is not the case because such a change would be observed across all antennas simultaneously, as they all see the same sky signal. Since we tend to see only a few antennas change significantly on any given night, if any, it seems clear that a changing polarization state of the incident radiation can be ruled out as the cause. Further, this suggests that the cross-feed correlation is indeed dominated by the Stokes-I term, or else we would see simultaneously night-to-night variations across all antennas.

7 Direct Testing

It might be useful to establish directly the sensitivity of the CCC to known changes in an antenna's structure.

8 A Interesting RFI Event

While inspecting the data from JD 2459122 I stumbled upon an RFI event at LST ∼4hr and ∼150MHz, in channel 844 and 845. The time series for the CCC, and for the auto/cross-correlations for two antennas are shown in Figure 17 The event is interesting because it has a profile in the CCC that looks like a source transiting the array over about 15 minutes and because of the large change in amplitude in both real and imaginary parts. According to HERA Memo #7 the International Space Station transmits at 149.75±55MHz, and its angular speed is approximately 4 degrees per minute, which is roughly consistent with the length of the pulse seen in the HERA data. Note both the amplitude and shape of the CCC for this transit. The oscillation between signs is reminiscent of the Stokes-I instrumental response kernel of the cross-feed correlations. On the other hand the fact that the CCC approaches 1 and the large imaginary part is probably indicative of a strongly polarized source - which a transmitter would be.

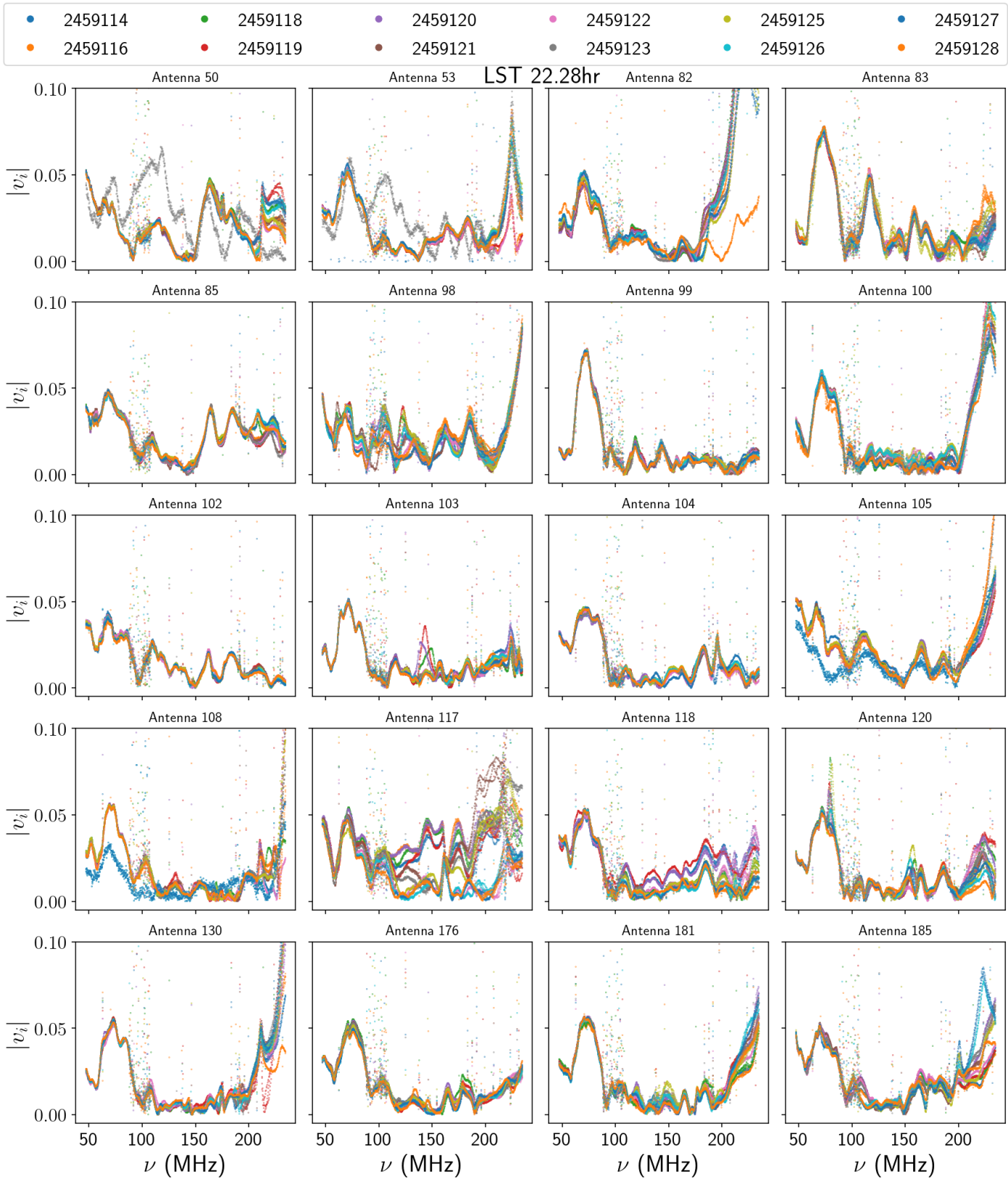

Figure 8: Variation between several days in the H4C season of the CCC amplitude for 20 different antennas.

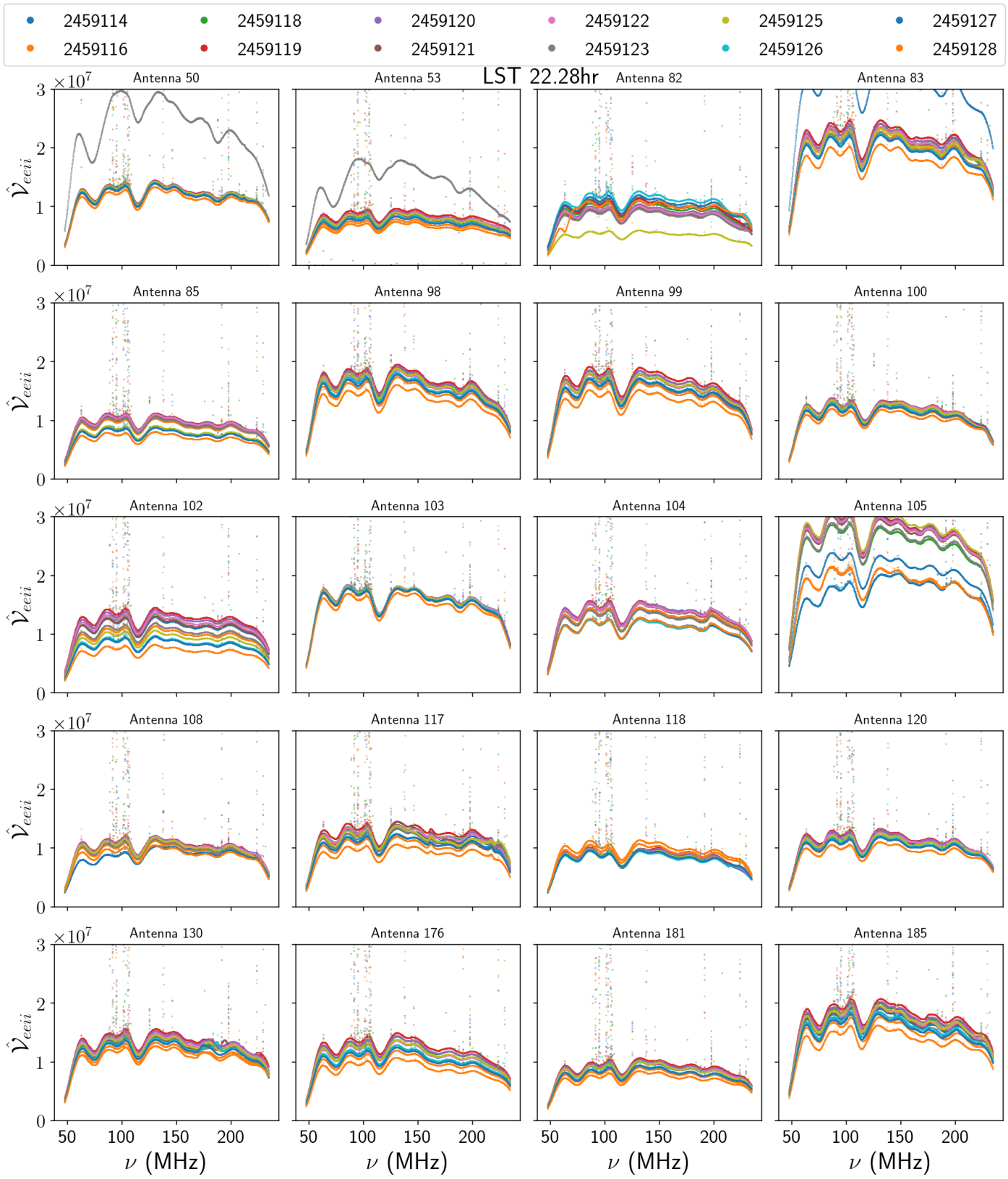

Figure 9: Variation between several days in the H4C season of the ee auto-correlation for 20 different antennas.

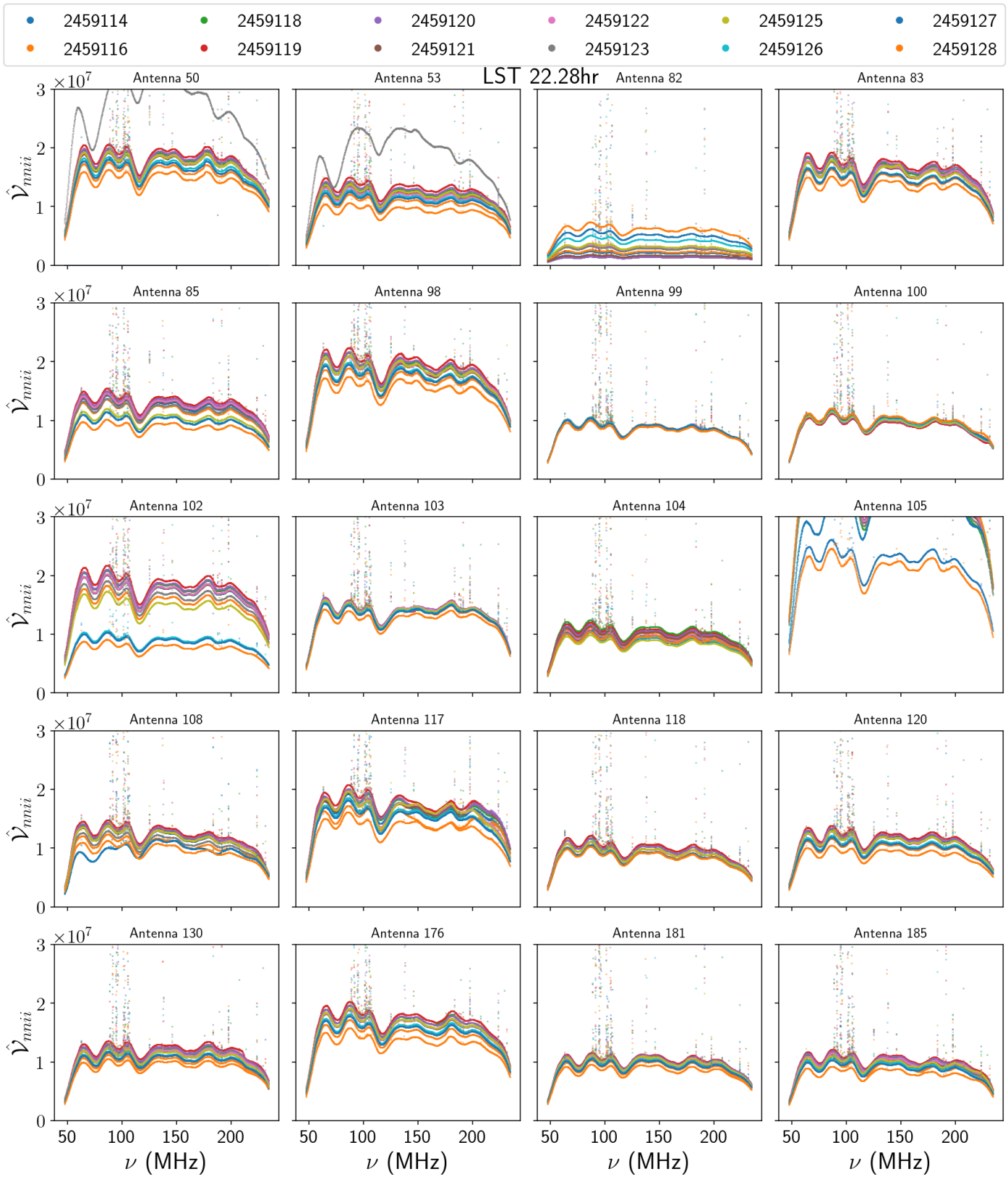

Figure 10: Variation between several days in the H4C season of the nn auto-correlation for 20 different antennas.

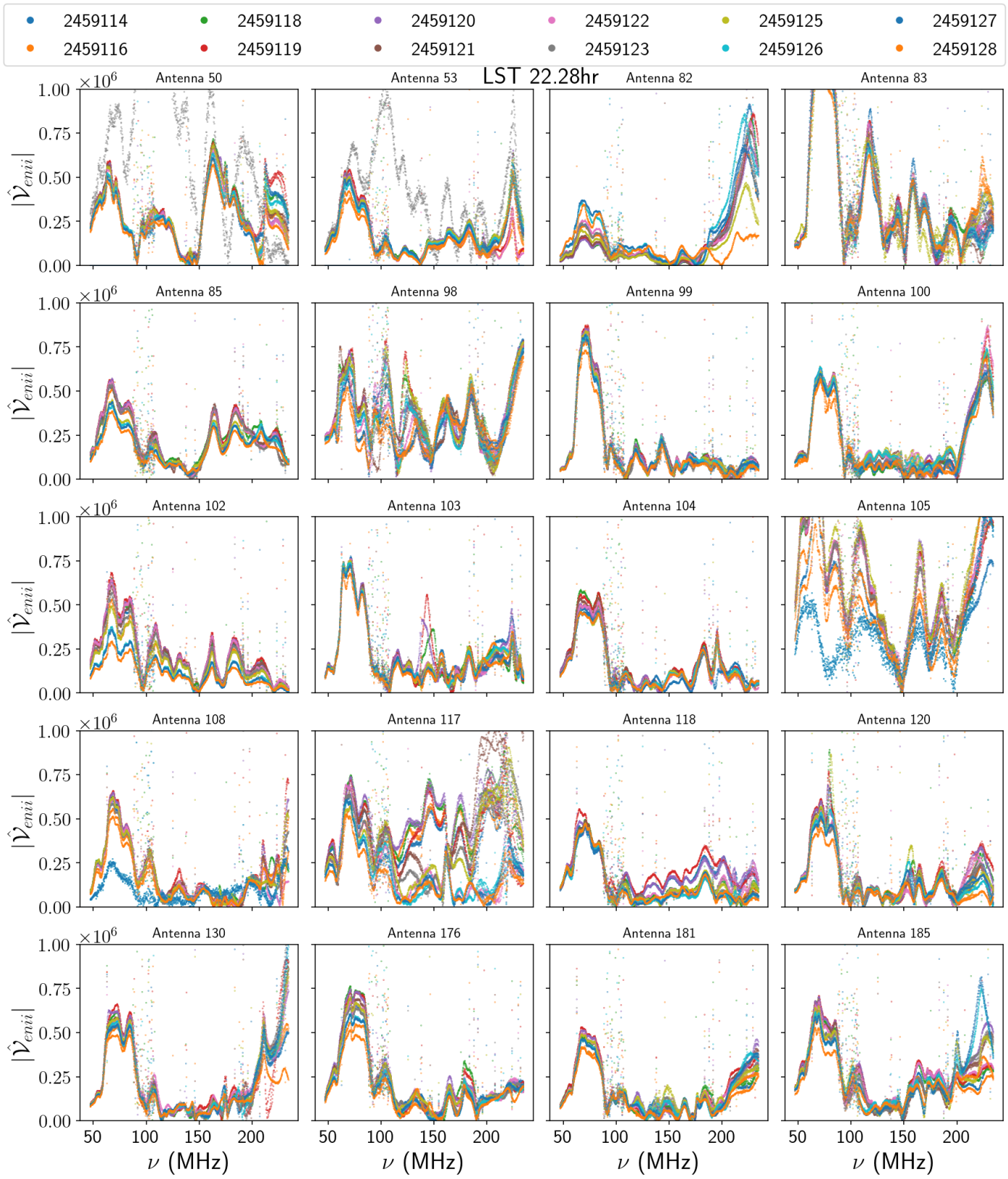

Figure 11: Variation between several days in the H4C season of the cross-feed correlation for 20 different antennas.

Figure 12: Variation between several days in the H4C season of the CCC amplitude for 20 different antennas.

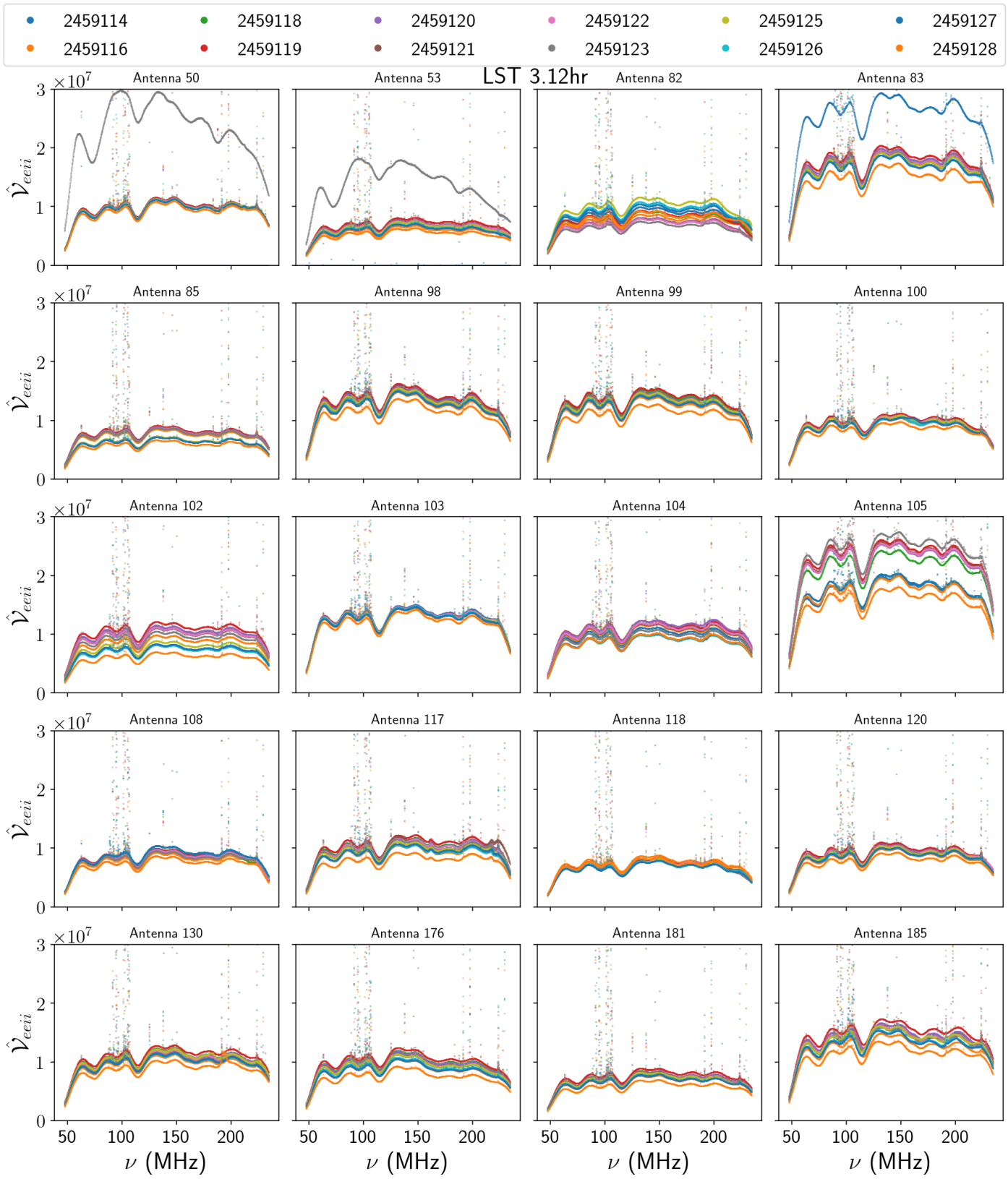

Figure 13: Variation between several days in the H4C season of the ee auto-correlation for 20 different antennas.

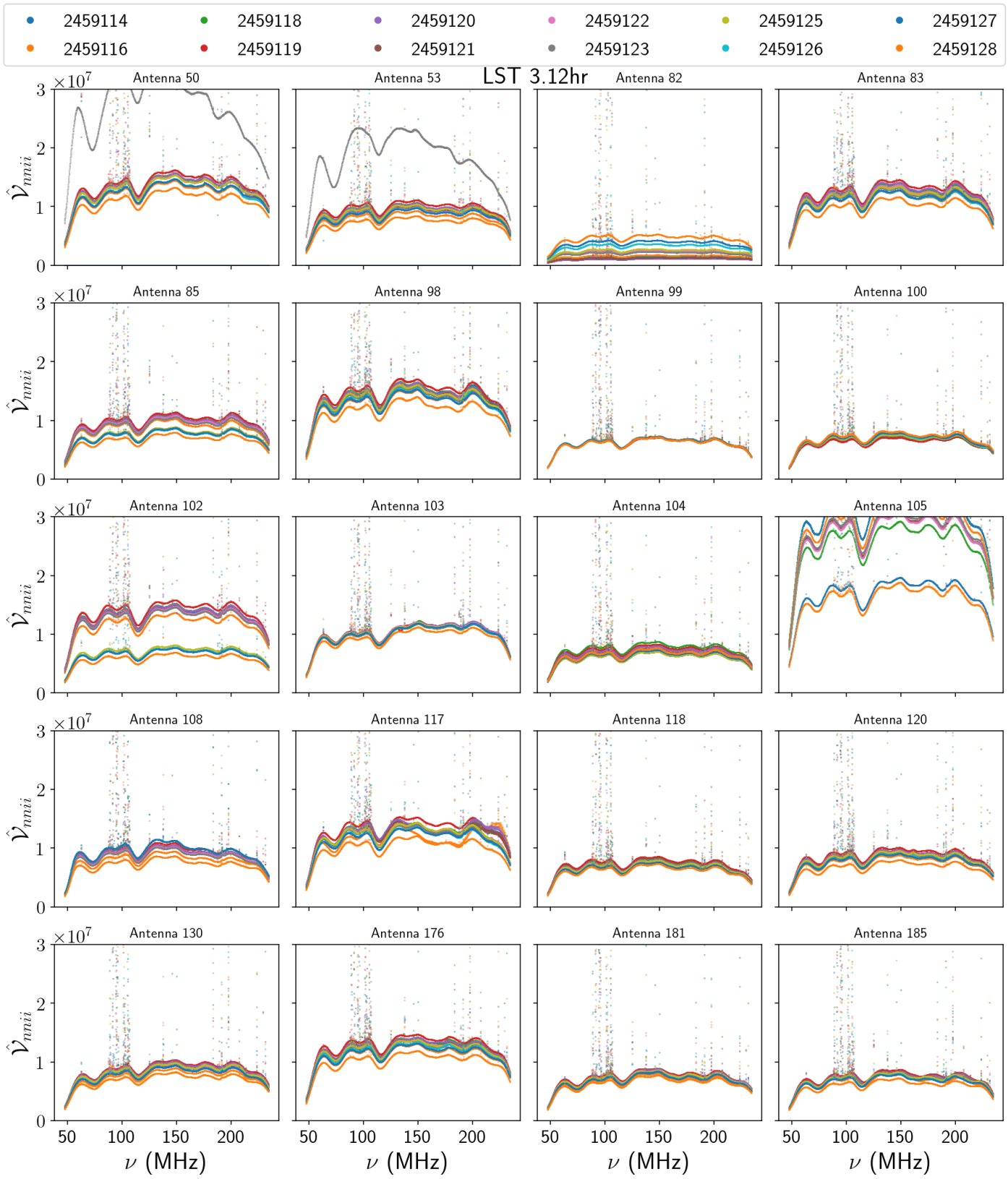

Figure 14: Variation between several days in the H4C season of the nn auto-correlation for 20 different antennas.

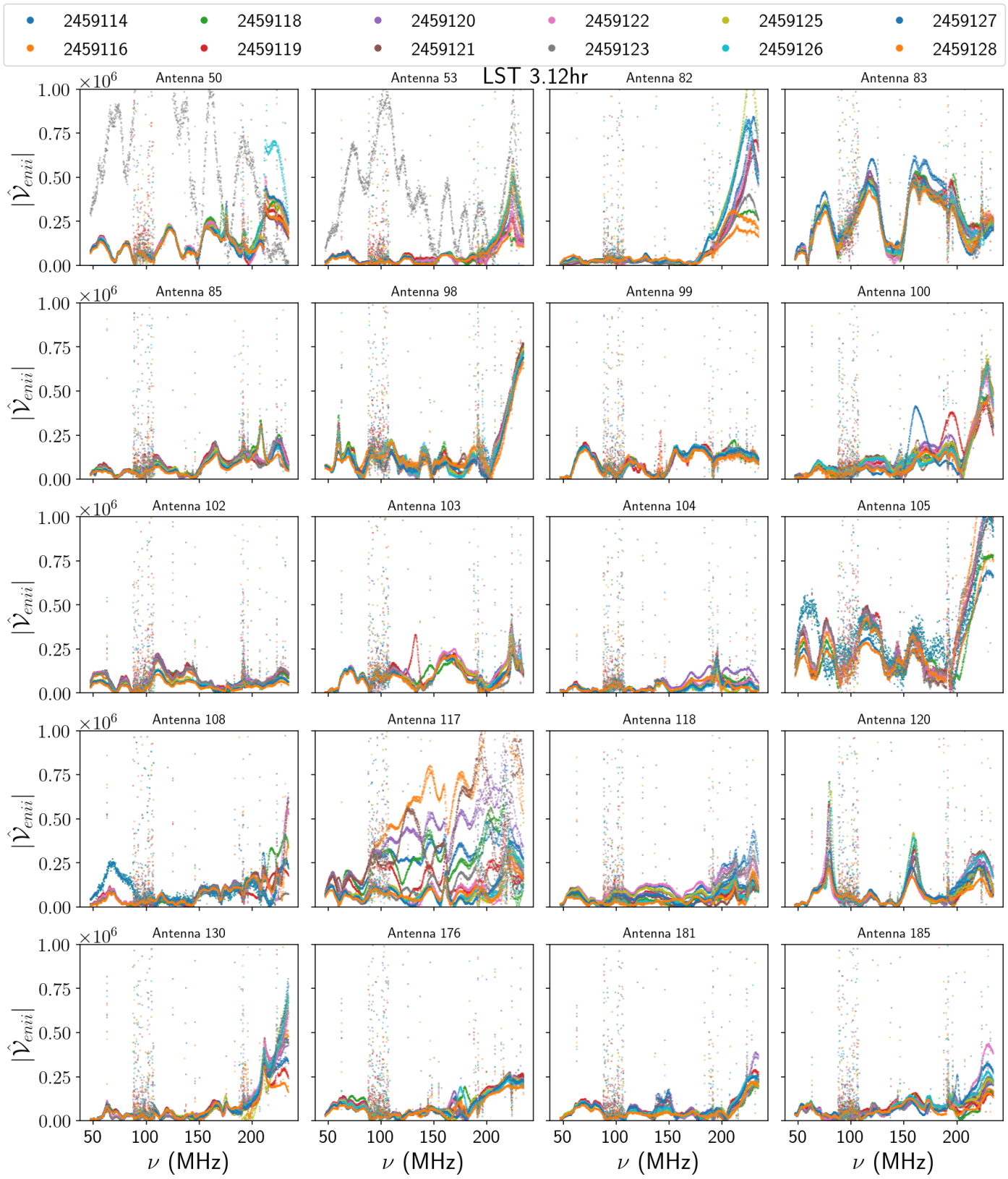

Figure 15: Variation between several days in the H4C season of the cross-feed correlation for 20 different antennas.

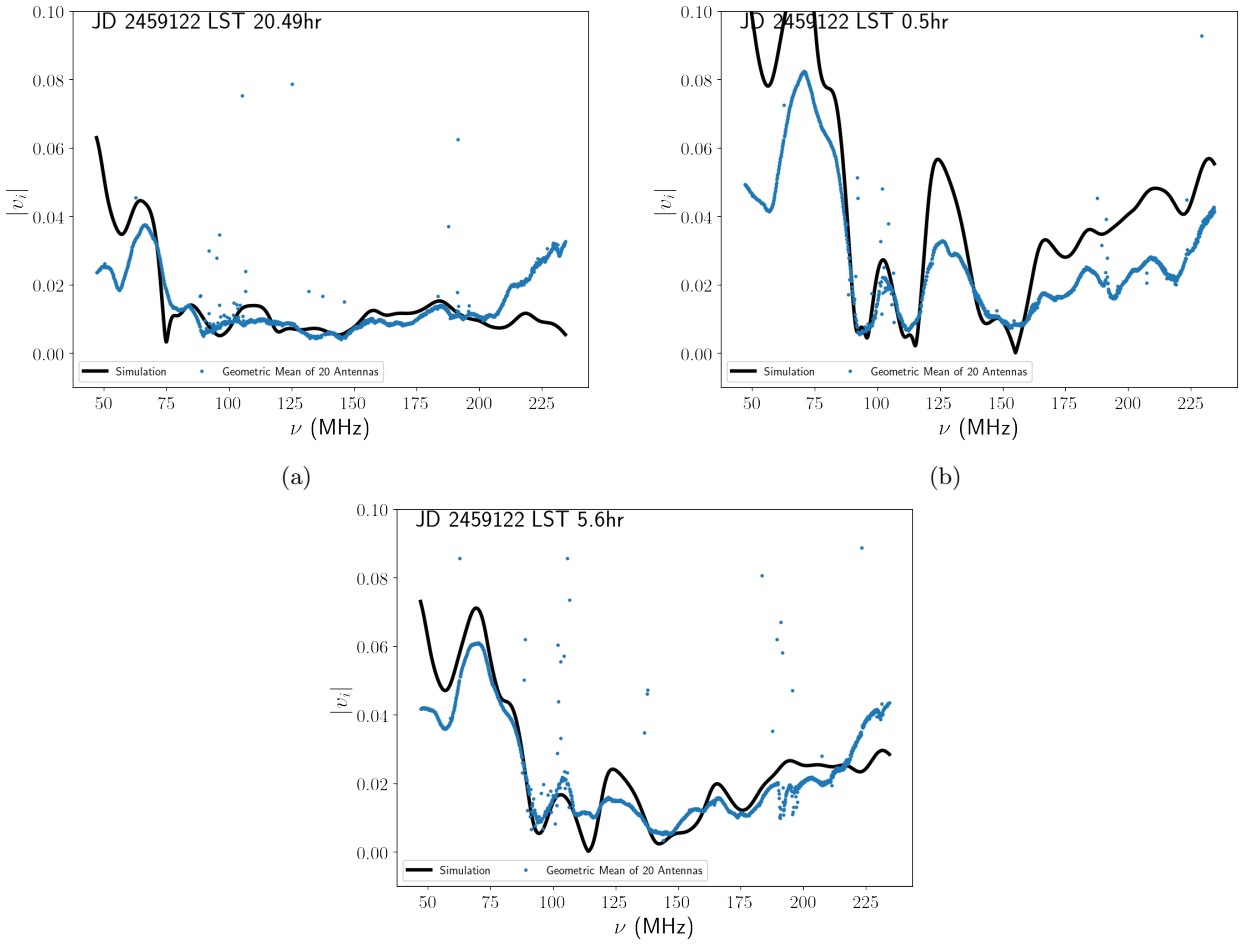

(a) (b)

(c)

Figure 16: Comparision of the mean spectrum of the 20 antennas to the simulation.

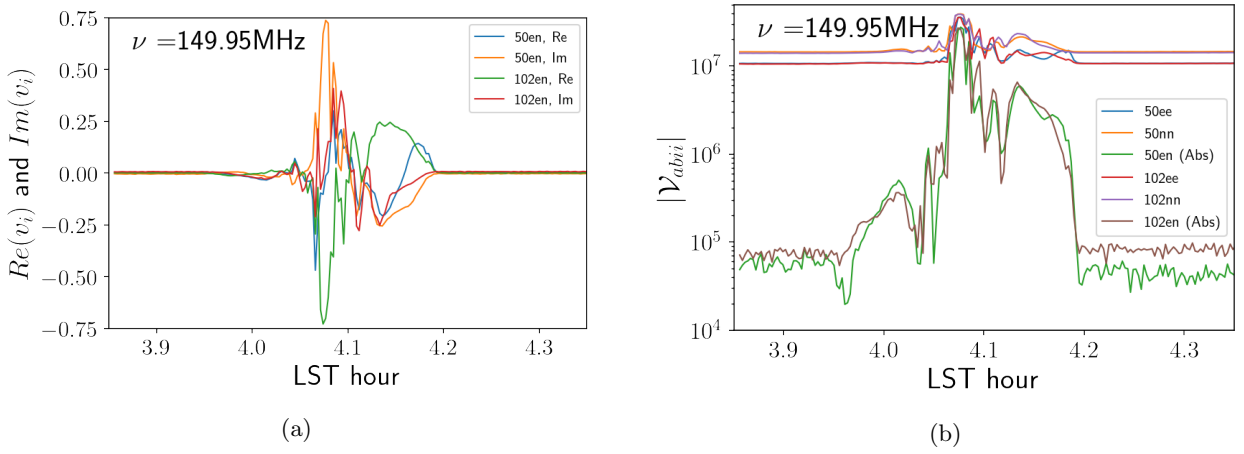

(a) (b)

Figure 17: Time series showing what appears to be a transit of the International Space Station in the CCC and auto/cross-feed correlations on JD 2459122. Note in (b) how the cross-feed correlation increases dramatically to approach the magnitude of the auto-correlations, which comes about when the incident emission is highly polarized.